Monthly Notices of the ROYAL ASTRONOMICAL SOCIETY

MNRAS **523,** 2850–2857 (2023) https://doi.org/10.1093/mnras/stad1438
Advance Access publication 2023 May 12

MeerKAT caught a Mini Mouse: serendipitous detection of a young radio pulsar escaping its birth site

S. E. Motta [1,2★] J. D. Turner,[3] B. Stappers [3] R. P. Fender,[2] I. Heywood,[2,4,5] M. Kramer[6] and E. D. Barr [6]

[1]*Istituto Nazionale di Astrofisica, Osservatorio Astronomico di Brera, via E. Bianchi 46, I-23807 Merate (LC), Italy*
[2]*Astrophysics Sub-department, Department of Physics, University of Oxford, Denys Wilkinson Building, Keble Road, Oxford OX1 3RH, UK*
[3]*Jodrell Bank Centre for Astrophysics, Department of Physics and Astronomy, The University of Manchester, Manchester M13 9PL, UK*
[4]*Department of Physics and Electronics, Rhodes University, PO Box 94, Makhanda 6140, South Africa*
[5]*South African Radio Astronomy Observatory, 2 Fir Street, Observatory 7925, South Africa*
[6]*Max-Planck-Institut fur Radioastronomie, Auf dem Hügel 69, D-53121 Bonn, Germany*

Accepted 2023 May 8. Received 2023 May 8; in original form 2023 March 22

ABSTRACT

In MeerKAT observations pointed at a Galactic X-ray binary located on the Galactic plane, we serendipitously discovered a radio nebula with cometary-like morphology. The feature, which we named 'the Mini Mouse' based on its similarity with the previously discovered 'Mouse' nebula, points back towards the previously unidentified candidate supernova remnant G45.24+0.18. We observed the location of the Mini Mouse with MeerKAT in two different observations, and we localized with arcsecond precision the 138-ms radio pulsar PSR J1914+1054g, recently discovered by the FAST telescope, to a position consistent with the head of the nebula. We confirm a dispersion measure of about 418 pc cm^{-3} corresponding to a distance between 7.8 and 8.8 kpc based on models of the electron distribution. Using our accurate localization and two period measurements spaced 90 d apart, we calculate a period derivative of $(2.7 \pm 0.3) \times 10^{-14}$ s s^{-1}. We derive a characteristic age of approximately 82 kyr and a spin-down luminosity of 4×10^{35} erg s^{-1}. For a pulsar age comparable with the characteristic age, we find that the projected velocity of the neutron star is between 320 and 360 km s^{-1} if it was born at the location of the supernova remnant. The size of the proposed remnant appears small if compared with the pulsar characteristic age; however, the relatively high density of the environment near the Galactic plane could explain a suppressed expansion rate and thus a smaller remnant.

Key words: accretion, accretion discs – black hole physics – stars: jets – pulsars: individual: PSR J1914+1054g – X-rays: binaries.

1 INTRODUCTION

Pulsar wind nebulae (PWNe) are the result of the interaction between the relativistic particle winds produced by rotationally powered pulsars and the surrounding medium. The rapid rotation of the magnetic field of the neutron star (NS) powers a relativistic wind, which, via interaction with the ambient medium, generates a termination shock downstream of which synchrotron radiation emerges with a spectrum extending from the radio band up to the γ-rays (see e.g. Gaensler & Slane 2006, for a review). Sometimes, a PWN is surrounded by a shell-like supernova remnant (SNR), legacy of the explosion that gave birth to the pulsar itself, and in this case the system is termed 'composite' (Matheson & Safi-Harb 2005).

If a pulsar moves through the interstellar medium (ISM) at a supersonic speed, a bow shock forms, which redirects and channels the pulsar wind in the direction opposite to that of the pulsar's motion. This may result in a detectable tail that can extend for several parsecs behind the NS (see e.g. Kargaltsev et al. 2015). In such cases, the SNR associated with the formation of the NS may be located parsecs away from the PWN, although the cometary tail may either connect to or point in the direction of the supernova shell. Among the several tens of PWNe known, only a small number of objects present such a cometary morphology, which is indicative of high proper velocities and/or a dense ISM. High spatial resolution observations in radio and X-ray bands are adding to this group (e.g. Klingler et al. 2018).

Detailed studies of the PWNe and their pulsars can provide crucial information on these systems, as the PWNe's appearance, spectrum, and radiative efficiency depend on the pulsars' parameters (e.g. spin, spin-down power, and surface magnetic field and its orientation), on the pulsars' velocity, and on the properties of the pulsar wind (e.g. flow speed and magnetization). Additionally, since PWNe have a well-defined central engine and are often close enough to be resolvable with high angular resolution observations, they represent excellent laboratories for studying both relativistic particle winds and the shocks that result when such outflows collide with the ISM, thus offering the opportunity to constrain the properties of their environment.

As part of the ThunderKAT Large Survey programmepro, which is aimed at providing a long-term view of interesting transients in the radio band, we observed the field of the black hole binary GRS 1915+105 with the MeerKAT radio telescope at *L* band with a few

★ E-mail: sara.motta@inaf.it

arcsec angular resolution (Motta et al. 2021).In the MeerKAT field of the source, we identified a feature that closely resembles 'the Mouse' (Yusef-Zadeh & Bally 1987), a radio nebula with axial symmetry, consisting of a bright 'head' and a long 'tail', observed in the direction of the Galactic Centre region, which hosts the young radio pulsar PSR J1747−2958 (Camilo et al. 2002). Based on the resemblance with the Mouse, we named the newly identified feature in the GRS 1915+105 field 'the Mini Mouse'.

This paper is structured as follows. In Section 2, we describe the imaging and time-domain data acquisition. In Section 3, we report the discovery of the Mini Mouse, the identification of PSR J1914+1054g, recently discovered by FAST, as the counterpart, and calculate the spin period derivative. Finally, in Section 4, we discuss the inferred nature of the Mini Mouse from these measurements.

2 OBSERVATIONS AND DATA ANALYSIS

2.1 Continuum observations

We observed the field of GRS 1915+105 61 times with MeerKAT as part of the ThunderKAT Large Survey Project (Fender et al. 2016) between 2018 December and 2022 April. We observed at a central frequency of 1.28 GHz across a 0.86-GHz bandwidth (856–1712 MHz). The correlator delivered either 4096 or 32 768 channels, with an 8-s integration time per visibility point, which were binned down to 1024 channels for consistency before any further analysis. Between 58 and 64 of the 64 available dishes were used in the observations, with a maximum baseline of 7.698 km. Of 61 observations, 60 consisted of 15 min of on-source time, book-ended by two 2-min scans of the secondary calibrator J2011−0644, plus a 10-min observation of a primary calibrator (J1939−6342; Motta et al. 2021). One observation lasted 90 min, of which 60 min were on-source, 20 min on the primary calibrator, and 3 min on the secondary calibrator.

Imaging was conducted via a set of PYTHON scripts specifically tailored for the semi-automatic processing of MeerKAT data (OxKAT[1]; Heywood 2020). Initial flagging to remove the first and final 100 channels from the observing band, autocorrelations, zero-amplitude visibilities, and radio frequency interference (RFI) was performed in CASA (McMullin et al. 2007). Further flagging was performed using the TRICOLOUR package,[2] after averaging the data in time (8 s) and frequency (eight channels) for imaging purposes. We imaged the field of GRS 1915+105 using WSCLEAN (Offringa, van de Gronde & Roerdink 2012) and combining the visibilities from all our observations after uv-subtracting the variable emission from GRS 1915+105. Direction-independent self-calibration was performed using CUBICAL (Kenyon et al. 2018) by solving for phase and delay corrections for every 32 s of data.

2.2 Search for a pulsar counterpart

The most sensitive pulsar search previously conducted that covered the position of the Mini Mouse is the ongoing FAST Galactic Plane Pulsar Snapshot (GPPS) survey (Han et al. 2021), with a 10σ sensitivity threshold between 1 and 10 μJy for periods of 10^{-2} and 10 s. The FAST GPPS survey recently discovered a faint (S_{1400} = 33 μJy) pulsar, PSR J1914+1054g (hereafter J1914) with a spin period of 138 ms, and a position consistent with the head of the Mini Mouse within a 1.5-arcmin uncertainty (Han et al. 2021).

In order to confirm the association between either J1914 or an undiscovered pulsar and the Mini Mouse head, we conducted a 2-h observation (henceforth referred to as OBS1, see Table 1) as part of the TRAPUM Large Survey Project (Stappers & Kramer 2016) with a nominal 10σ sensitivity of 10.6 μJy. We observed at a central frequency of 1284 MHz and a bandwidth of 856 MHz (identical to that used in the continuum observations), split into 4096 channels, with a sampling time of 153 × 10^{-6} s. We used all 64 available dishes, which gives the minimum coherent beam (CB) size. A CB is formed by coherently summing the digitized signals from each receiver after correcting for the geometric delay, and accesses a much smaller field of view than the primary (incoherent) beam does. The on-site Filterbank and BeamForming User-Supplied Equipment (FBFUSE) computer cluster, developed by the Max-Planck-Institüt für Radioastronomie (Barr 2017), uses the beamforming package MOSAIC[3] to derive a set of delay polynomials that will synthesize multiple CBs. This enables the tessellation of hexagonally packed beams across a source (Chen et al. 2021). For OBS1, 266 beams were arranged in a rectangle overlapping at their 75 per cent power width, to densely cover the full length and breadth of the nebula. The beam at the centre of the field of view was placed on the head of the Mini Mouse at the position of largest continuum flux. Additional 66 beams were used to tile over the portion of the 1.5-arcmin position error region that was not covered by the rectangle.

Approximately 45 min into the observation, a failure of one of the eight capture nodes of the Accelerated Pulsar Search User Supplied Equipment (APSUSE) resulted in ensuing data being corrupted in some beams. The observation was suspended a short time later. Luckily, the seven most central beams positioned on the head of the Mini Mouse were unaffected, yielding 104 min of good data. The corresponding filterbanks were processed offline to search for J1914 directly before any global periodicity search was attempted.

Raw data are recorded on the APSUSE file system in the SIGPROC[4] filterbank format, segmented by beam and in 5-min chunks. The initial search for J1914 was conducted first on the innermost beam as it is located both at the point of maximum sensitivity (boresight) and at the position of maximum flux of the nebula's head. The `filtool` program, which is part of PULSARX,[5] was used to clean RFI and to stitch together the continuous data into a single filterbank file. Using PSRCHIVE's DSPSR (Van Straten & Bailes 2011), the filterbank file was folded using an ephemeris containing J1914's period and the dispersion measure (DM) for the epoch reported in Han et al. (2021). CLFD[6] was then applied to the full-resolution folded data to clean any lingering RFI. Finally, a search over period and DM was performed with `pdmp` (Hotan, Van Straten & Manchester 2004; Van Straten & Bailes 2011) with a window of 50 μs in period and 20 units of DM. The observation yielded a detection of J1914 with a significance of 19.4 in the beam directly placed on the Mini Mouse head, with P = 138.867 651 ms and a DM of 418.0 ± 0.3 pc cm^{-3}. As a result of this detection at the head of the nebula, no full-scale periodicity search of all CBs was attempted. Using the spin period measured

[1] https://github.com/IanHeywood/oxkat
[2] https://github.com/ska- sa/tricolour/
[3] https://github.com/wchenastro/Mosaic by Weiwei Chen.
[4] http://sigproc.sourceforge.net/
[5] https://github.com/ypmen/PulsarX by Yunpeng Men.
[6] https://github.com/v-morello/clfd by Vincent Morello.

Table 1. A summary of the observing parameters and resources used for the two MeerKAT observations of J1914.

Parameter	OBS1	OBS2
UTC start time (yyyy-MM-dd-hh:mm:ss)	2022-08-03-21:03:30	2022-11-01-16:54:47
Start MJD	59794.877431	59884.704630
Duration (s)	6296	7186
Number of dishes	64	62
Central frequency (MHz)	1284	1284
Bandwidth (MHz)	856	856
Channels	4096	4096
Sampling time (s)	156×10^{-6}	72×10^{-6}
Right ascension[a] (hh:mm:ss)	19:14:09.46	19:14:09.66
Declination[a] (dd:mm:ss)	+10:54:43.7	+10:54:42.2

[a]The value refers to the coordinates of the central CB.

Table 2. Measured and inferred quantities for J1914 derived from OBS2. The value in brackets denotes the 1σ uncertainty on the rightmost digit.

Measured quantities	
Right ascension, α (J2000)	$19^{\rm h}14^{\rm m}09\overset{\rm s}{.}83^{+0.41}_{-0.12}$
Declination, δ (J2000)	$+10^\circ54'35\overset{''}{.}9^{+13.4}_{-2.0}$
Pulse period, P (s)	0.138 867 860(17)
Pulse period derivative, $\dot{P}$ (s s^{-1})	$2.7(3) \times 10^{-14}$
Duty cycle (per cent)	14
Dispersion measure, DM (pc cm^{-3})	418.90(26)
Flux density, S_{1284} (μJy)	62.1
Inferred quantities	
Distance (NE2001) (kpc), d_1	7.8
Distance (YMW16) (kpc), d_2	8.8
Characteristic age, $\tau_{\rm c}$ (kyr)	82(11)
Surface dipole magnetic field strength, B (G)	$1.9(1) \times 10^{12}$
Spin-down luminosity, $\dot{E}$ (erg s^{-1})	$4.0(6) \times 10^{35}$
Radio pseudo-luminosity, L_{1284} at d_1 (mJy kpc^2)	3.8
X-ray luminosity, $L_{\rm X}(1-10\,{\rm keV})$ at d_1 (erg s^{-1})	$<7 \times 10^{32}$

by the FAST telescope about 2 yr before,[7] we estimated a tentative period derivative of about 3×10^{-14} s s^{-1}.

In order to obtain a second accurate measurement of the spin period of J1914 with MeerKAT, and to meaningfully constrain the spin derivative, we requested and obtained a Director's Discretionary Time (DDT) observation of the Mini Mouse position (henceforth OBS2, project code DDT-20221028- SM-01, see Table 1). Only seven beams at 75 per cent overlap were required to cover J1914's position derived from OBS1. The optimal tiling pattern selected by MOSAIC is a central beam surrounded by a hexagon of six, a configuration suited for signal-to-noise ratio-based localization techniques. The reduction in the number of beams also allowed for observing at a time resolution of 76×10^{-6} s. These data were reduced and searched in the same way as in OBS1. The observing parameters and resources used for both observations are summarized in Table 2.

3 RESULTS

An image of the MeerKAT field is shown in Fig. 1, which also includes a zoom into the Mini Mouse. The Mini Mouse appears as a long structure extending from position RA, Dec. $19^{\rm h}14^{\rm m}09\overset{\rm s}{.}5$, $+10^\circ54'42\overset{''}{.}7$ for over 5 arcmin in the east-north-east direction, with a flux density varying along its axis between about 0.08 and 0.2 mJy beam^{-1} (marked by a rectangle in Fig. 1). Unlike the original Mouse, the Mini Mouse does not have an obviously extended head at the MeerKAT resolution of 6.6 arcsec, and remains unresolved in the transverse direction for its entire length, albeit brighter in the first 2 arcmin than in the tail. Further observations at higher angular resolution and/or higher frequency will help to clarify the finer angular scale structure of this nebula.

Our continuum radio map shows several bright extended structures, including H II regions and several shell-like non-thermal radio structures, many of which can be associated with SNRs. One such structure is located to the east-north-east of the Mini Mouse, and is a previously unidentified dim, remarkably circular SNR candidate G45.24+0.18 (marked by a circle in Fig. 1). The geometrical centre of the SNR is located within 30 arcsec from the extension of the Mini Mouse axis of symmetry, and 12 arcmin away from the head of the Mini Mouse. The SNR has an apparent radius of 5.7 arcmin and a flux density of 20–40 μJy beam^{-1}.

We detected J1914 in OBS2, this time with a significance of 24.3σ, as can be seen in Fig. 2. The results of the detection and analysis to be discussed hereafter are reported in Table 2. Using the difference in period, ΔP, and time, Δt, between OBS1 and OBS2, we derive for the first time[8] the period derivative, $\dot{P} = \Delta P/\Delta t$, of J1914 to

[7]The period measured by FAST was kindly provided by Prof. JinLin Han via private communication.

[8]FAST published the timing of one single visit to J1914, based on which a first estimate of the pulsar period was made (Han et al. 2021). The period derivative could not be estimated based on one single observation.

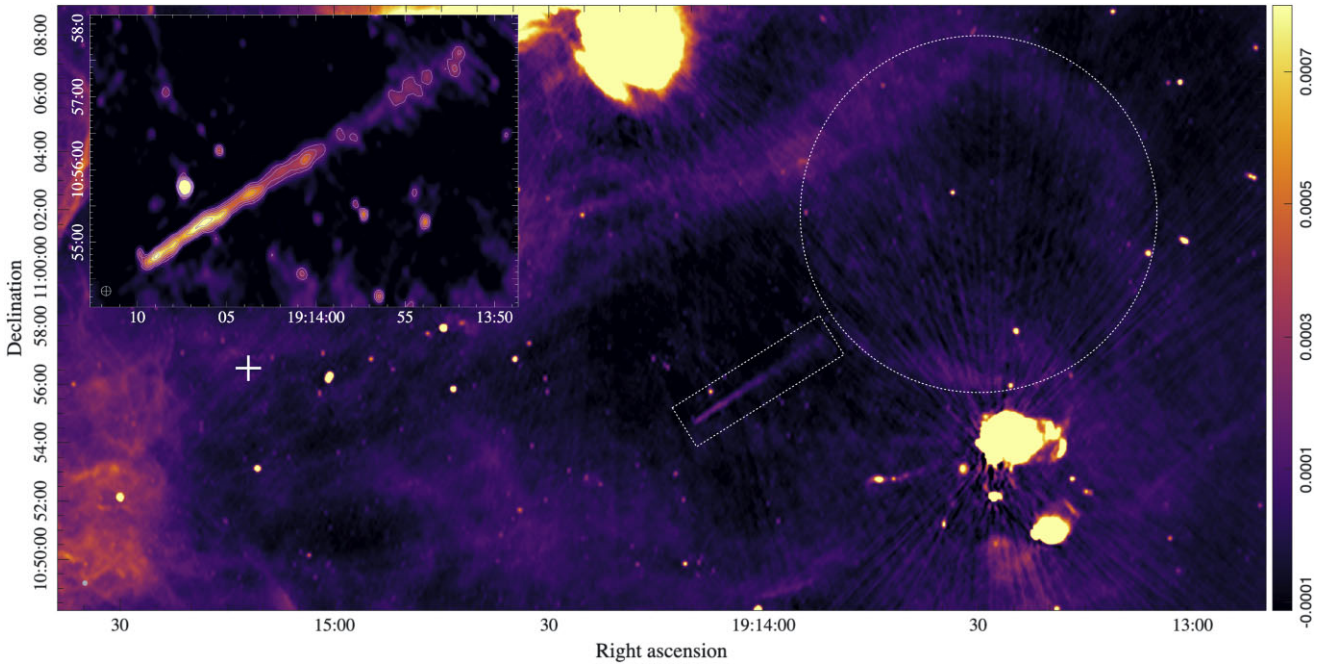

Figure 1. A portion of the field centred on GRS 1915+105 as seen by the MeerKAT radio telescope at 1.28 GHz. The total on-source time is 15.5 h. The restored beam for this map is circular and has a radius of 6.6 arcsec, shown in the bottom-left corner of the image. The Mini Mouse and the SNR associated with the birth of pulsar J1914 are marked by a rectangle and a circle, respectively. The location of GRS 1915+105 is marked by a cross. Inset: A zoom into the Mini Mouse. Contours are equally spaced, and span the range 10–200 uJy. The 'tooth' at the edge of the nebula is likely a background source.

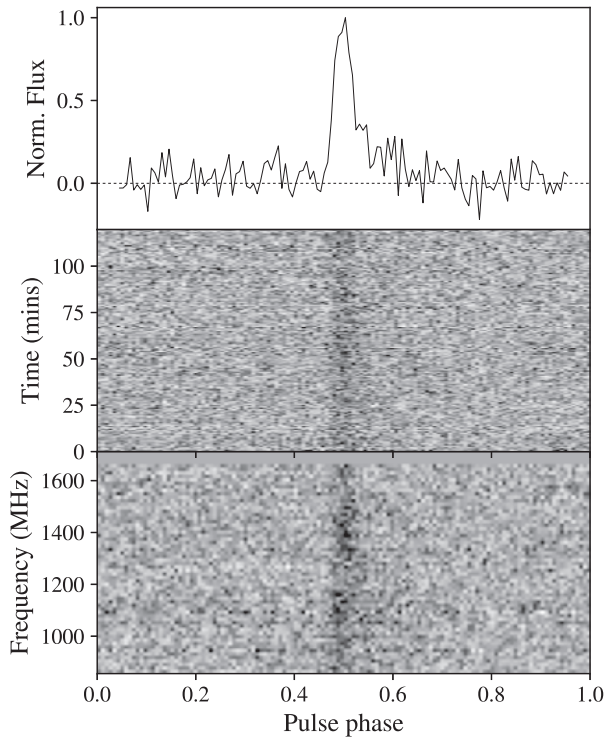

Figure 2. Second MeerKAT detection of J1914 folded at the best period and dedispersed. Bottom panel: Frequency against pulse phase across the band with a resolution of 128 channels. Middle panel: Band-integrated time series for the 2-h observation showing the flux for each 2-min subintegration. Top panel: Integrated pulse profile made by stacking the time series into 128 bins. Evidence for scattering in the ISM can be seen in the asymmetric broadening of the pulse profile.

be 2.7(3) $\times$ 10^{-14} s s^{-1}. Using both the NE2001 (Cordes & Lazio 2002) and YMW16 (Yao, Manchester & Wang 2017) electron density models, we find the distance for a DM of 418.9 pc cm^{-3} to be d_1 $\sim$ 7.8 and d_2 $\sim$ 8.8 kpc, respectively, with the usual caveat of large uncertainties associated with this method. This distance range places J1914 (and thus the Mini Mouse) in the same region of the Galaxy hosting the black hole binary GRS 1915+105 ($8.6^{+2.0}_{-1.6}$ kpc; Reid et al. 2014). At the above distance, the Mini Mouse has a projected length between 11.9 and 13.4 pc, and the SNR that we tentatively associated with the pulsar birth has a radius between 12.8 and 14.4 pc (assuming that the remnant is spherically symmetrical).

3.1 Localization

Given a flux density of 62.1 μJy and an rms noise of about 50–55 μJy, we do not expect J1914 to be identifiable as a point source in the image here. However, we are able to localize J1914 to arcsecond accuracy using SEEKAT,[9] the PYTHON implementation of Tied Array Beam Localizer (Bezuidenhout et al. 2023), which is used to localize pulsars discovered by both the TRAPUM and MeerTRAP[10] projects (see Bezuidenhout et al. 2022; Vleeschower et al. 2022, for respective examples). SEEKAT implements a novel method of maximum-likelihood estimates using the S/N in each CB and a model of the point spread function (PSF) from MOSAIC. The PSF changes shape and orientation as the source moves through the sky (Chen et al. 2021), so we model it at the observation mid-point. The beams used for the localization are shown in the left-hand panel of Fig. 3. The S/N in each beam was obtained by folding the data with DSPSR using an ephemeris of the best period and DM for the

[9]https://github.com/BezuidenhoutMC/SeeKAT by Mechiel C. Bezuidenhout.
[10]More TRAnsients and Pulsars with MeerKAT.

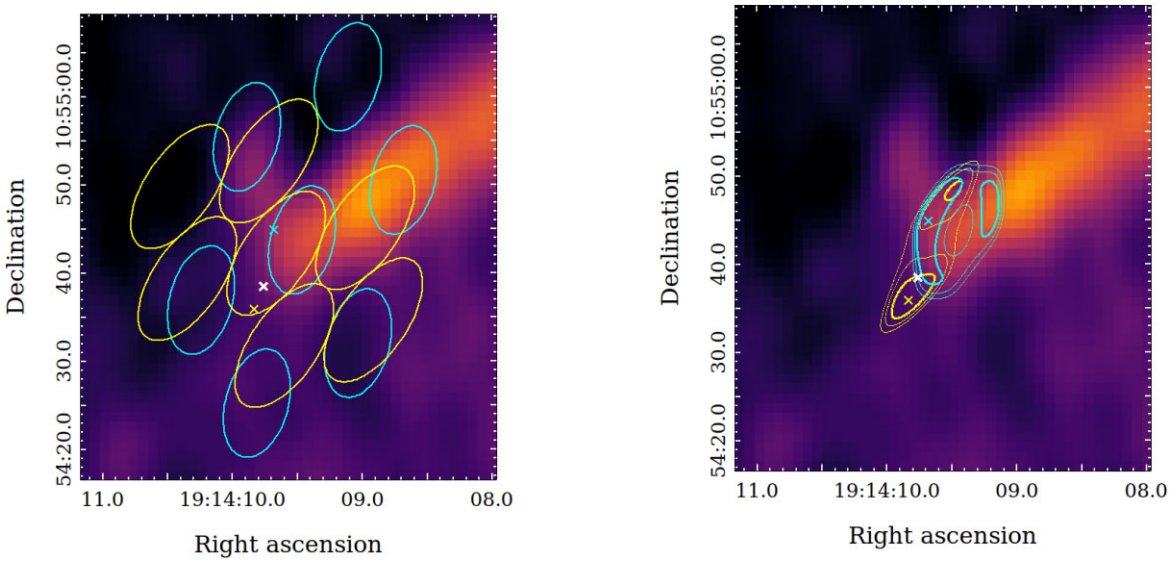

Figure 3. The OBS1 (cyan) and OBS2 (yellow) localization of J1914 from SEEKAT. The crosses indicate the maximum-likelihood position. The bold white cross is the weighted mean of the two positions. The ellipses (left) are the 75 per cent power radii of the CBs. The contours (right) are the 1σ (bold), 2σ, and 3σ levels of the likelihood fit.

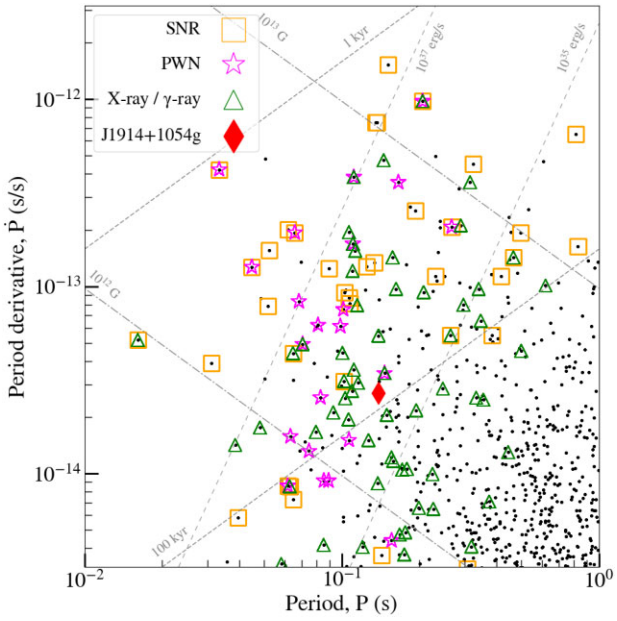

Figure 4. A plot of $\dot{P}$ against P for the young pulsar populace, J1914 inclusive. The canonical radio pulsars emerge towards the lower right of the plot. Pulsars with confirmed associations with SNRs, PWNe, or detections at high energies, according to the ATNF catalogue (Manchester et al. 2005), are indicated, as are the contour lines for B, τ_c, and $\dot{E}$.

observation epoch, before reducing these folded data to a single subintegration and frequency channel and obtaining the S/N using the `psrstat` command. The results from SEEKAT are shown in the right-hand panel of Fig. 3. The position quoted in Table 2 is the OBS2 result because the S/N is higher than OBS1. The weighted mean position of OBS1 and OBS2 is also shown for discussion purposes.

S/N values in OBS1 disfavour a position within the beam directly on the nebula head, and instead indicate that it lies on its north-western edge, towards a little spur that may or may not be noise. The analysis of OBS2 yields a bimodal likelihood, seemingly the result of probability leakage towards the gaps in the CB ring.[11] There is an island of 1σ contour overlap very close to the weighted mean position, although both still appear in front of the nebula.

3.2 Period derivative significance

As mentioned in Section 3, we had two MeerKAT epochs that were not phase connected and we used the period and its uncertainty, and standard error propagation to calculate $\dot{P} = 2.7(3) \times 10^{-14}$ s s^{-1}. However, this calculation assumes that the period errors are the dominant source of uncertainty. In order to verify such an assumption, we calculated other contributions to the uncertainty on $\dot{P}$. First, we estimated the error in the pulse arrival time at the Earth due to an assumed position error. The Römer delay correction for an erroneous source position changes the apparent spin period as the Earth moves in its orbit (see e.g. Lorimer & Kramer 2005; Edwards, Hobbs & Manchester 2006). In the worst-case scenario, the period is measured at the closest and furthest positions from the source on the ecliptic sphere. Using the largest 1σ error on RA and Dec. from Table 2 of 6.2 and 13.4 arcsec and assuming these are approximately equivalent to the uncertainty in ecliptic longitude and latitude, the maximum change in arrival time is 43.4 ms. This yields an apparent change in period of 3.8×10^{-10} s over the 6 months, which would translate into a negligible additional $\dot{P}$ of 2.4×10^{-17} s s^{-1}.

Another small apparent change in P could be caused by the Doppler effect from the transverse motion of the pulsar as projected on the celestial sphere, which is known as the Shklovskii effect

[11] MOSAIC's default is to pack beams within a circular region. Unfortunately, the six-beam hexagon has gaps due to the ellipticity of the CBs. Care should have been taken when planning OBS2 to make sure the source was observed closer to the zenith, as more circular CBs would better enclose the central beam.

(Shklovskii 1970). We estimate that the upper limit of this effect may induce an apparent $\dot{P}$ of $\sim 7 \times 10^{-20}$ s s^{-1}, which is much smaller than our uncertainty, and thus can be ignored.

3.3 X-ray serendipitous observations

The position of J1914 was observed serendipitously by the Neil Gerhels Swift Observatory (*Swift*) for a total of 8.3 ks, although no source is detected significantly according to the *Swift*-XRT LSXPS Upper limit server (Evans et al. 2023). We derived an upper limit to the 1–10-keV X-ray flux of approximately 8×10^{-14} erg cm^{-2} s^{-1}, assuming a blackbody spectrum with temperature 2 keV and an equivalent column density in the direction of the source of 1.36×10^{22} cm^{-3}.

4 DISCUSSION

In the MeerKAT observations of the black hole binary GRS 1915+105, we discovered an unusual collimated linear nebula, which based on the similarity with the Mouse feature found in the '80s in the direction of the Galactic Centre (Yusef-Zadeh & Bally 1987), we named *the Mini Mouse*. At a distance of 12 arcmin from the Mini Mouse head, we also identified a circular feature that we classify as a candidate SNR based on its morphology, the apparent centre of which is found in the direction indicated by the tail of the Mini Mouse. The relative positions of the Mini Mouse and of the faint candidate remnant are strongly reminiscent of three similar nebulae with radio pulsar engines: the original Mouse (Yusef-Zadeh & Bally 1987; Camilo et al. 2002), the 'Frying Pan' (Kesteven et al. 1987; Camilo et al. 2009) nebula, and the 'Cannon ball' pulsar PSR J0002+6216 (Schinzel et al. 2019; Kumar et al. 2023). All three systems have an accompanying SNR, which have been associated with the birth of the escaping pulsars. Such a resemblance motivated our pulsar search.

Our MeerKAT observations localize J1914 with an accuracy of approximately 10 arcsec to a position fully consistent with the head of the Mini Mouse, hence supporting a physical association. Thus, we interpret the Mini Mouse nebula as the bow shock produced by the pulsar escaping at supersonic speed through the local ISM away from its birth location. Synchrotron radiation emerges from the pulsar relativistic wind interacting in the nebular magnetic field, similar to what was concluded for the case of the aforementioned Mouse, Frying Pan, and cannon-ball nebulae.

Although the J1914 is localized on the head of the Mini Mouse, its position lies on the north-western edge of it rather than to the centre of the head. In principle, we do not expect the pulsar to be in front of the radio emission, as the bow shock is formed ahead of the wind termination shock at the boundary where the ram pressure of the ISM equals that of the PWN (e.g. Kargaltsev et al. 2017). However, the ISM likely has pronounced density variability based on the flux variation along the tail in Fig. 1, so it is possible that the pulsar is moving into a higher density pocket and the distance between the two shocks is shrinking. An alternative explanation could be that there may be emission on smaller angular scales here that is being missed in the image. Finally, the discrepancy between the continuum map and the pulsar localization inferred from the timing could be explained in terms of a systematic positional offset that may affect MeerKAT images, and is generally of the order of 1–2 arcsec or larger (e.g. Mauch et al. 2020). High angular resolution observations of the Mini Mouse will clarify this issue.

Our position uncertainty has an area of 7.5×10^{-6}. The Mini Mouse is directly in the centre of the first Galactic plane quadrant at $l = 45^\circ$ and $b = 0^\circ$. The region bound by $0^\circ < l < 90^\circ$ and $|b| < 2.5^\circ$ contains 910 pulsars, giving a rough probability of chance alignment of 1.5×10^{-5}, and hence we are confident that the Mini Mouse nebula is the result of J1914 in motion.

The MeerKAT data yielded a period P and period derivative $\dot{P}$ of 138 ms and $2.7(3) \times 10^{-14}$ s, respectively, for J1914, which imply a spin-down luminosity $\dot{E} = 4\pi^2 I \dot{P}/P^3 = 4.0(6) \times 10^{35}$ erg s^{-1} (where $I = 10^{45}$ g cm^2 is the NS moment of inertia), a characteristic age $\tau_c = P/2\dot{P} = 82$ kyr, and surface magnetic dipole field strength $B = 3.2 \times 10^{19}(P\dot{P})^{1/2} = 2.1 \times 10^{12}$ G. These parameters place J1914 near the young and energetic pulsars in the P–$\dot{P}$ diagram (see Fig. 4), characterized by an average spin-down luminosity $\dot{E} \sim 10^{36}$ erg s^{-1}, and a characteristic age τ_c ranging from 10 to 100 kyr. Given the upper limit to the X-ray luminosity of the Mini Mouse, assuming isotropic emission, we obtain an upper limit to the X-ray luminosity of $L_X < 7 \times 10^{32}$ erg s^{-1}, and thus an upper limit to conversion efficiency of the spin-down luminosity into X-ray emission of $L_X/\dot{E} < 1.5 \times 10^{-3}$. The non-detection is not surprising as this limit is a factor of about 6 higher than the limit estimated for the 'Frying Pan pulsar', which is also undetected in X-rays (Camilo et al. 2009).

If we assume that the pulsar's actual age is approximately equal to its characteristic age (which is not necessarily true; see Gaensler & Frail 2000), the SNR should be approximately 80 kyr old. At such an age, a typical remnant in a low-density ambient medium is expected to have entered the snowplough expansion phase, having transitioned from the Sedov–Taylor adiabatic expansion phase about 50 kyr after detonation (see Jiménez, Tenorio-Tagle & Silich 2019, and references therein). In the snowplough phase, the radio shell should have a very low surface brightness Σ and large diameter D according to the Σ–D inverse relationship (see e.g. Vukotić et al. 2019). At our DM-based distances, the SNR shell would have a diameter of 12.8 or 14.4 pc, which is more typical of a remnant in the mid-to-late Sedov–Taylor phase, with an age of about 20 kyr. Such a discrepancy can be explained if the ISM is sufficiently dense (Frail, Goss & Whiteoak 1994), as efficient radiative cooling from expansion into a high-density ambient medium can inhibit the Sedov–Taylor phase, a plausible scenario given that this remnant is located on the Galactic plane (see e.g. Terlevich et al. 1992; Jiménez et al. 2019). We note that the distance derived from the DM measure might not be accurate, and hence we could in principle decide to ignore it and instead derive the distance from the Σ–D relation. However, this method has often been treated with scepticism due to possible intrinsic biases in the correlation, and in particular due to the fact that (i) the Σ–D relation is derived from independently determined distances, which each have their own uncertainties (Green 1991), and (ii) SNRs show a diversity of intrinsic properties, for example the population of SNRs in the LMC that are roughly all the same distance from Earth (Green 1984). Therefore, we decided to wait for additional information on the source to make this attempt.

Again assuming that the pulsar characteristic age of 82 kyr is close to the pulsar actual age, and that the faint circle of emission is the progenitor remnant, we can obtain an estimate of the pulsar's transverse velocity component, $v_\perp$, by considering the distance between the centre of the SNR and the head of the Mini Mouse. For a pulsar distance of 7.8 or 8.8 kpc, the resulting projected pulsar velocity is between 320 and 360 km s^{-1}, which is well within the kick velocity distribution for young, isolated pulsars, centred at approximately 300 km s^{-1}, with a dispersion of approximately 190 km s^{-1} (Hansen & Phinney 1997).

If the connection between J1914 and the faint SNR is correct, then we may have a faint, fast-spinning, distant young pulsar with a high kick velocity, i.e. a member of an undersampled population, which could help extrapolating the local young pulsar velocity distribution to the wider Galactic one (Hansen & Phinney 1997). Under the assumption that the magnetic moment of the pulsar remains constant, the actual age and the characteristic age of a pulsar are connected by the relation $\tau = \tau_c[1 - (P_0/P)^{n-1}]/(n - 1)$, where P_0 is the pulsar spin period at birth and n is the breaking index of rotation (Manchester et al. 1978). Using the standard assumptions of $P_0 \ll P$ and $n = 3$ in the case of magnetic dipole breaking (see e.g. Camilo et al. 2002, for the case of the Mouse pulsar) and $\tau = \tau_c$, the above relation implies that P_0 is between 10 and 20 ms, which is consistent with the expected theoretical values for a newborn radio pulsar and thus supports our hypothesis of a young and fast-spinning pulsar.

5 SUMMARY AND CONCLUSIONS

In the MeerKAT data dedicated to the monitoring of a Galactic X-ray binary, we found a radio nebula, which we named 'the Mini Mouse'. Such a feature is produced by a supersonic pulsar escaping the location of its birth, marked by the presence of the faint and previously unknown SNR candidate G45.24+0.18 also discovered in the MeerKAT data. Time-domain observations found the signal from a radio pulsar in correspondence of the tip of the Mini Mouse, confirming the association of the nebula with a previously poorly localized faint pulsar discovered by the FAST telescope, J1914+1054g.

The Mini Mouse is the fourth case of a bow shock associated with an escaping pulsar, for which both the pulsar signal and the SNR associated with its birth have been observed. Additional high angular resolution observations of the Mini Mouse will clarify its finer scale structure, and will bring a better characterization of the local ISM, while additional high time-resolution observations of J1914+1054g will significantly improve the timing solution, thus providing a better constraint on the pulsar properties.

The ThunderKAT discovery of the Mini Mouse and the TRAPUM confirmation of the association with J1914+1054g constitute an excellent example of immense potential of the MeerKAT data. Thanks to the detection of structures similar to the Mouse and Mini Mouse, MeerKAT will help unveiling more young radio pulsars that will add to the still small population of such objects, which is predicted to count thousands of members in our Galaxy (e.g. Lorimer et al. 1993).

ACKNOWLEDGEMENTS

The authors thank the anonymous referee who reviewed this work providing useful suggestions to improve it. SEM acknowledges JinLin Han for providing the spin period of PSR J1914+1054g from the FAST GPPS, and Lauren Rhode for comments on an early version of this work. SEM acknowledges financial contribution from the agreement ASI-INAF n.2017-14-H.0 and from the INAF mainstream grant. JDT acknowledges funding from the United Kingdom's Research and Innovation Science and Technology Facilities Council. All the authors thank the staff at the South African Radio Astronomy Observatory (SARAO) for scheduling the MeerKAT observations presented here. TRAPUM observations used the FBFUSE and APSUSE computing clusters for data acquisition, storage, and analysis. These clusters were funded and installed by the Max-Planck-Institüt für Radioastronomie (MPIfR) and Max-Planck-Gesellschaft. The MeerKAT telescope is operated by the South African Radio Astronomy Observatory, which is a facility of the National Research Foundation, an agency of the Department of Science and Innovation. SAOImage DS9 was used for image analysis and presentation.

DATA AVAILABILITY

The uncalibrated MeerKAT visibility data presented in this paper are publicly available in the archive of the South African Radio Astronomy Observatory at https://archive.sarao.ac.za. The continuum MeerKAT observations were taken as part of the ThunderKAT Large Survey programme, project code SCI-20180516-PW-01. The project code for the TRAPUM Science Working Group collaborated with is SCI-20180923-MK-03, and for the DDT observation is DDT-20221028-SM-01. Data that are not available through public archives, and all source codes, will be shared on reasonable request to the corresponding author.

REFERENCES

Barr E. D., 2017, in Weltevrede P., Perera B. B. P., Preston L. L., Sanidas S., eds, Proc. IAU Symp. 337, An S-Band Receiver and Backend System for MeerKAT Cambridge University Press, Proceedings of the International Astronomical Union. p. 175.
Bezuidenhout M. C. et al., 2022, MNRAS, 512, 1483
Bezuidenhout M. C. et al., 2023, preprint (arXiv:2302.09812)
Camilo F., Manchester R. N., Gaensler B. M., Lorimer D. R., Sarkissian J., 2002, ApJ, 567, L71
Camilo F., Ng C. Y., Gaensler B. M., Ransom S. M., Chatterjee S., Reynolds J., Sarkissian J., 2009, ApJ, 703, L55
Chen W., Barr E., Karuppusamy R., Kramer M., Stappers B., 2021, J. Astron. Instrum., 10, 2150013
Cordes J. M., Lazio T. J. W., 2002, preprint (astro-ph/0207156)
Edwards R. T., Hobbs G. B., Manchester R. N., 2006, MNRAS, 372, 1549
Evans P. A., Page K. L., Beardmore A. P., Eyles-Ferris R. A. J., Osborne J. P., Campana S., Kennea J. A., Cenko S. B., 2023, MNRAS, 518, 174
Fender R. et al., 2016, in Proceedings of MeerKAT Science: On the Pathway to the SKA. Stellenbosch, South Africa (MeerKAT2016). https://pos.sissa.it/cgi-bin/reader/conf.cgi?confid=277, id.13.
Frail D. A., Goss W. M., Whiteoak J. B. Z., 1994, ApJ, 437, 781
Gaensler B. M., Frail D. A., 2000, Nature, 406, 158
Gaensler B. M., Slane P. O., 2006, ARA&A, 44, 17
Green D. A., 1984, MNRAS, 209, 449
Green D. A., 1991, PASP, 103, 209
Han J. L. et al., 2021, Res. Astron. Astrophys., 21, 107
Hansen B. M. S., Phinney E. S., 1997, MNRAS, 291, 569
Heywood I., 2020, Astrophysics Source Code Library, record ascl:2009.003
Hotan A. W., Van Straten W., Manchester R. N., 2004, Publ. Astron. Soc. Aust., 21, 302
Jiménez S., Tenorio-Tagle G., Silich S., 2019, MNRAS, 488, 978
Kesteven M. J., Caswell J. L., Roger R. S., Milne D. K., Haynes R. F., Wellington K. J., 1987, Aust. J. Phys., 40, 855
Kargaltsev O., Cerutti B., Lyubarsky Y., Striani E., 2015, Space Sci. Rev., 191, 391
Kargaltsev O., Pavlov G. G., Klingler N., Rangelov B., 2017, J. Plasma Phys., 83, 635830501
Kenyon J. S., Smirnov O. M., Grobler T. L., Perkins S. J., 2018, MNRAS, 478, 2399
Klingler N., Kargaltsev O., Pavlov G. G., Ng C. Y., Beniamini P., Volkov I., 2018, ApJ, 861, 5
Kumar P., Schinzel F. K., Taylor G. B., Kerr M., Castro D., Rau U., Bhatnagar S., 2023, ApJ, 945, 129

Lorimer D. R., Kramer M., 2005, A Handbook of Pulsar Astronomy. Cambridge Univ. Press, Cambridge
Lorimer D. R., Bailes M., Dewey R. J., Harrison P. A., 1993, MNRAS, 263, 403
Manchester R. N., Lyne A. G., Taylor J. H., Durdin J. M., Large M. I., Little A. G., 1978, MNRAS, 185
Manchester R. N., Hobbs G. B., Teoh A., Hobbs M., 2005, AJ, 129, 1993
Matheson H., Safi-Harb S., 2005, Adv. Space Res., 35, 1099
Mauch T. et al., 2020, ApJ, 888, 61
McMullin J. P., Waters B., Schiebel D., Young W., Golap K., 2007, in Shaw R. A., Hill F., Bell D. J., eds, ASP Conf. Ser. Vol. 376, Astronomical Data Analysis Software and Systems XVI. Astron. Soc. Pac., San Francisco, p. 127
Motta S. E. et al., 2021, MNRAS, 503, 152
Offringa A. R., van de Gronde J. J., Roerdink J. B. T. M., 2012, A&A, 539, A95
Reid M. J., McClintock J. E., Steiner J. F., Steeghs D., Remillard R. A., Dhawan V., Narayan R., 2014, ApJ, 796, 2
Schinzel F. K., Kerr M., Rau U., Bhatnagar S., Frail D. A., 2019, ApJ, 876, L17
Shklovskii I., 1970, Sov. Astron., 13, 562
Stappers B. W., Kramer M., 2016, in Proceedings of MeerKAT Science: On the Pathway to the SKA. Stellenbosch, South Africa, https://pos.sissa.it/cgi-bin/reader/conf.cgi?confid=277, id.9
Terlevich R., Tenorio-Tagle G., Franco J., Melnick J., 1992, MNRAS, 255, 713
Van Straten W., Bailes M., 2011, Publ. Astron. Soc. Aust., 28, 1
Vleeschower L. et al., 2022, MNRAS, 513, 1386
Vukotić B., Ćiprijanović A., Vučetić M. M., Onić D., Urošević D., 2019, Serb. Astron. J., 199, 23
Yao J. M., Manchester R. N., Wang N., 2017, ApJ, 835, 29
Yusef-Zadeh F., Bally J., 1987, Nature, 330

This paper has been typeset from a TEX/LATEX file prepared by the author.